Published in final edited form as:

Cell Host Microbe. 2016 July 13; 20(1): 13–24. doi:10.1016/j.chom.2016.05.011.

RIPK3 activates parallel pathways of MLKL-driven necroptosis and FADD-mediated apoptosis to protect against influenza A virus

Shoko Nogusa[1,*], **Roshan J. Thapa**[1,*], **Christopher P. Dillon**[2,*], **Swantje Liedmann**[2], **Thomas H. Oguin III**[2], **Justin P. Ingram**[1], **Diego A. Rodriguez**[2], **Rachelle Kosoff**[1], **Shalini Sharma**[2], **Oliver Sturm**[2], **Katherine Verbist**[2], **Peter J. Gough**[3], **John Bertin**[3], **Boris M. Hartmann**[4], **Stuart C. Sealfon**[4], **William J. Kaiser**[5], **Edward S. Mocarski**[5], **Carolina B. López**[6], **Paul G. Thomas**[2], **Andrew Oberst**[7,*,#], **Douglas R. Green**[2,#], and **Siddharth Balachandran**[1,#]

[1]Blood Cell Development and Function Program, Fox Chase Cancer Center, Philadelphia, PA, 19111 USA

[2]Department of Immunology, St. Jude Children's Research Hospital, Memphis, TN, 38105 USA

[3]Pattern Recognition Receptor Discovery Performance Unit, Immuno-Inflammation Therapeutic Area, GlaxoSmithKline, Collegeville, PA, 19426 USA

[4]Department of Neurology, Icahn School of Medicine at Mt. Sinai, New York, NY, 10029 USA

[5]Emory Vaccine Center, Emory University, Atlanta, GA, 30322 USA

[6]School of Veterinary Medicine, University of Pennsylvania, Philadelphia, PA, 19104 USA

[7]Department of Microbiology and Immunology, University of Washington, Seattle, WA, 98109 USA

Summary

Influenza A virus (IAV) is a lytic virus in primary cultures of many cell types and *in vivo*. We report that the kinase RIPK3 is essential for IAV-induced lysis of mammalian fibroblasts and lung epithelial cells. Replicating IAV drives assembly of a RIPK3-containing complex that includes the kinase RIPK1, the pseudokinase MLKL, and the adaptor protein FADD, and forms independently of signaling by RNA-sensing innate immune receptors (RLRs, TLRs, PKR), or the cytokines type I interferons and TNF-α. Downstream of RIPK3, IAV activates parallel pathways of MLKL-driven

*Equal contribution.

#Co-senior authors: S.B., Room 224 Reimann Building, 333 Cottman Ave., Philadelphia, PA 19111, Phone: 215-214-1527. Fax: 215-728-3574. siddharth.balachandran@fccc.edu

D.R.G., 262 Danny Thomas Place, Memphis, TN 38105, Phone: 901-595-3488. Fax: 901-595-5766. douglas.green@stjude.org

Author Contributions. SN, RJT, CD, SL, THO, JPI, DAR, RK, SS, OS, KV, BMH and SCS performed experiments and analyzed data. PJG and JB developed and supplied RIPK1 and RIPK3 kinase inhibitors. WJK, ESM, and CBL provided reagents and intellectual input. PGT, AO, DRG and SB conceived the study and designed the experiments. SB wrote the manuscript. All authors participated in editing the manuscript.

Conflict of interest. Peter J. Gough and John Bertin are employees of GlaxoSmithKline.

necroptosis and FADD-mediated apoptosis, with the former reliant on RIPK3 kinase activity and neither on RIPK1 activity. Mice deficient in RIPK3 or doubly-deficient in MLKL and FADD, but not MLKL alone, are more susceptible to IAV than their wild-type counterparts, revealing an important role for RIPK3-mediated apoptosis in antiviral immunity. Collectively, these results outline RIPK3-activated cytolytic mechanisms essential for controlling respiratory IAV infection.

Introduction

Influenza A virus (IAV), a member of the family *Orthomyxoviridae* and primary causative agent of influenza in birds and mammals, is an enveloped virus with a negative-sense, single-stranded, segmented RNA genome. Acute IAV infection is accompanied by lysis of infected primary epithelial cells and fibroblasts in culture, and by destruction of airway epithelia *in vivo*, indicative of an integral role for cell death in the virus life cycle, the immune response to this virus, or both (Sanders et al., 2011; Yatim and Albert, 2011). It has been proposed that cell death, mainly apoptosis, may represent a host defense mechanism that limits both virus spread and host immunopathology early in an infection (Vaux et al., 1994; Yatim and Albert, 2011). More recent evidence suggests that unbridled necrotic cell death *in vivo* can lead to severe degradation of bronchiolar epithelia and consequent mortality despite control of virus replication (Rodrigue-Gervais et al., 2014). Moreover, severe illness following infection with highly pathogenic H1N1 and H5N1 strains of IAV is well-correlated with pulmonary epithelial cell death and bronchioalveolar tissue damage arising from hyperactive immune and inflammatory responses to these strains (Brandes et al., 2013; Kash et al., 2006; Sanders et al., 2011). Thus, although epithelial cell death eliminates the infected cell to check virus spread, the mode of cell death, as well as its timing and magnitude, are each significant determinants of disease outcome during an acute IAV infection. Despite substantial study, the mechanisms by which IAV triggers cell death and the contribution of particular cell death pathways to the control or pathogenesis of IAV *in vivo* remain unclear.

Here, we show that RIPK3 is a dominant mediator of cell death after IAV infection of murine fibroblasts and alveolar epithelial cells. Replicating IAV activates RIPK3, which then triggers parallel pathways of MLKL-dependent necrosis and RIPK1/FADD/caspase 8-driven apoptosis, either of which are capable of mediating the lysis of infected cells in culture. RIPK3 deficiency increases susceptibility to IAV *in vivo*, as does compound loss of both apoptosis and necroptosis effector arms downstream of RIPK3. But strikingly, loss of only MLKL does not appreciably increase susceptibility to IAV, demonstrating an important role for RIPK3-activated apoptosis in host defense against IAV. These results identify RIPK3 as a key effector of IAV-triggered cell lysis, outline the mechanism by which RIPK3 induces cell death, and define critical roles for RIPK3-induced cell death pathways in controlling spread of an important human pathogen.

Results

RIPK3 is required for IAV-induced cell death in murine fibroblasts and lung epithelial cells

To examine the role of RIPK3 in IAV induced cell death, we infected early-passage murine embryo fibroblasts (MEFs) from *ripk3*$^{-/-}$ and littermate-control *ripk3*$^{+/+}$ mice with IAV strains Puerto Rico/8/1934 (PR8), Brisbane/59/2007, Brisbane/10/2007, and Perth/16/2009 and observed these cells over a time course of 36 h. PR8 (H1N1) is a commonly-used natural isolate of IAV, while Brisbane/59/2007 (H1N1), Brisbane/10/2007 (H3N2), and Perth/16/2009 (H3N2) and are seasonal strains of IAV. We also included in this analysis two strains of influenza B virus (IBV), Brisbane/60/2008 and Florida/4/2006. Each of these strains induced extensive cytopathic effect (CPE) and cell death in infected wild-type MEFs within 24 h (Fig. 1A, B). Remarkably, similarly-infected *ripk3*$^{-/-}$ MEFs were almost completely resistant to IAV- and IBV- induced CPE and cell death at this time point (>85% viability, Fig. 1A, B), indicating that activating RIPK3-mediated cell death is a common cytopathic feature of influenza viruses. Focusing on IAV for the rest of this study, we observed that the capacity of *ripk3*$^{-/-}$ MEFs to withstand IAV-induced lysis paralleled their resistance to cell death induced by the combination of TNF-α, cycloheximide, and the pan-caspase inhibitor zVAD (TCZ), an established trigger of necroptosis in MEFs (Fig. 1A, B), and was largely reversed by the re-introduction of RIPK3 expression (Fig. S1A). Using recombinant PR8 expressing GFP [PR8-GFP; (Manicassamy et al., 2010)], we found that *ripk3*$^{-/-}$ MEFs were neither defective in viral entry nor any less permissive to IAV than *ripk3*$^{+/+}$ MEFs: both genotypes displayed equivalent levels GFP-positivity 24 h.p.i. with PR8-GFP (Fig. 1C). In line with these observations, immunoblot analysis of viral protein expression in lysates prepared from *ripk3*$^{+/+}$ and *ripk3*$^{-/-}$ MEFs infected with PR8 over a 24 h time course revealed no evidence of either decreased infectivity or delayed kinetics of replication in cells lacking RIPK3 (Fig. 1D).

By 36 h.p.i., most (>80%) *ripk3*$^{+/+}$ MEFs infected with IAV (hereafter PR8) were dead, while approximately half the population of infected *ripk3*$^{-/-}$ MEFs remained alive (Fig. 1E). Similarly infected *ripk3*$^{-/-}$ treated with zVAD or additionally lacking the apoptosis effectors caspase 8 or FADD remained mostly alive at this time point, indicating that the delayed death seen in *ripk3*$^{-/-}$ MEFs was mediated by a residual RIPK3-independent FADD/caspase8-dependent pathway of apoptosis (Fig. 1F). Neither TNF-α or TRAIL-mediated mechanisms, either alone or in combination, appear to account for this pathway of RIPK3-independent apoptosis in IAV-infected MEFs (Fig. S1B, C).

To extend these analyses to a physiologically relevant cell type, we next asked if RIPK3-driven cell death is triggered in lung type I alveolar epithelial cells (AECs) following infection with IAV. Type I AECs are productively infected by IAV and represent an essential niche for the initial round of IAV replication in the human and murine lung (Rosenberger et al., 2014; Sanders et al., 2011). Employing the immortalized murine type I AEC cell line LET1 (Rosenberger et al., 2014), we first confirmed that type I AECs express RIPK3 and its essential cell death regulators, RIPK1, FADD, MLKL and caspase 8, at levels comparable to those found in MEFs (Fig. S2). Upon infection with PR8, LET1 cells showed clear evidence of CPE within 3 h, and succumbed to infection within 12 h.p.i. (Fig. 1G, left). CRISPR/

Cas9-mediated ablation of RIPK3 expression protected LET1 cells from PR8 (Fig. 1G, left), demonstrating that RIPK3-driven cell death mechanisms are conserved between MEFs and lung AECs. Notably, LET cells lacking RIPK3 produced significantly more progeny virions than control LET1 cells containing RIPK3, predictive of a prominent role for RIPK3-driven cell death in clearance of virus from the infected lung (Fig. 1G, right).

IAV replication results in assembly of a RIPK3 complex containing RIPK1, FADD and MLKL

A defining molecular feature of RIPK3 dependent cell death is the stimulus-driven formation of a molecular complex called the 'necrosome' comprising as its core phosphorylated forms of RIPK3 and RIPK1, together with FADD and MLKL (Chan et al., 2015; Cho et al., 2009). From the necrosome, RIPK3 can activate both necroptosis and apoptosis, depending on target availability (Cook et al., 2014) or RIPK3 activity (Mandal et al., 2014; Newton et al., 2014). To test if IAV induced formation of a necrosome, we immunoprecipitated RIPK3 from lysates of PR8-infected MEFs and examined immunoprecipitates for the presence of slower-mobility forms of phosphorylated RIPK1. PR8 activated necrosome formation to a significant extent, as did the combination of PR8+zVAD (Fig. 2A, left and middle panels). Like TNF-α (Fig. 2A, right panels), IAV infection also drove the recruitment of FADD and MLKL into the RIPK3-RIPK1 necrosome. As zVAD alone at this dose (25μM) did not induce detectable necrosome formation, and as the combination of PR8+zVAD stabilized the necrosome to allow more reliable detection of IAV-activated RIPK3-containing complexes over PR8 alone, we used this combination for our subsequent dissection of the molecular determinants of IAV-triggered RIPK3 complex formation.

We found that PR8 induced a RIPK3-RIPK1 complex in MEFs beginning at ~10 h.p.i., after the start of viral protein NS1 accumulation, which was detectable at ~6–8 h.p.i (Fig. 2B). Given that IAV-induced RIPK3 necrosome assembly was preceded by viral protein synthesis, we next tested if active transcription, translation, or viral genome replication was required for IAV-induced RIPK3 activation. Pre-treatment of MEFs with the RNA polymerase II inhibitor Actinomycin D [ActD, which also blocks IAV replication: host RNA polymerase II is needed for export of IAV mRNAs from the nucleus to the cytoplasm (Amorim et al., 2007)] or with an inhibitor of mRNA translation, cycloheximide (CHX), effectively prevented both viral replication and RIPK3-RIPK1 complex formation (Fig. 2C). Neither ActD nor CHX at these doses affected TNF-α-induced necrosome assembly [(Thapa et al., 2013) not shown]. The IAV nucleoprotein inhibitor nucleozin (Kao et al., 2010) also potently blocked RIPK3-RIPK1 association at doses that abrogated viral replication (Fig. 2C). Together, these results demonstrate that IAV replication drives activation of RIPK3.

Next, we employed kinase inhibitors specific for either RIPK1 [GSK'481 (Harris et al., 2016), GSK'963 (Berger et al., 2015), and Necrostatin-1 (Degterev et al., 2008)] or RIPK3 [GSK'872 and GSK'843 (Mandal et al., 2014)] to identify roles for the kinase activity of each of these proteins in IAV-induced RIPK3-RIPK1 complex assembly. Downstream of TNFR1, the kinase activity of RIPK1, but not RIPK3, was necessary for necrosome formation (Fig. 2D, left panels), although both classes of inhibitor were potent blockers of TNF-α-induced cell death (Fig. 3A). In contrast to how these kinases function in the TNF-α

pathway, we found that the kinase activity of RIPK3 was required for IAV-induced necrosome formation, while that of RIPK1 was largely dispensable (Fig. 2D, right panels). Thus, while RIPK3 complexes activated by TNF-α and IAV both contain RIPK1, FADD, and MLKL, and are licensed by caspase inhibition, they display contrasting requirements for the kinase activities of RIPK1 versus RIPK3.

Several innate-immune pathways are triggered by an acute RNA virus, many of which (e.g., TNF-α, type I IFNs, TLR3) have been shown to activate RIPK3 (Mocarski et al., 2014; Sridharan and Upton, 2014). To test if any of these pathways are responsible for necrosome formation and RIPK3-driven cell death in response to IAV infection, we infected primary MEFs deficient in either PKR, IFNAR1, STAT1, RIG-I, MAVS, TNFR1 or MyD88/TRIF, and monitored necrosome formation and RIPK3-dependent cell death in these cells. IFNAR1, STAT1 and PKR are required for type I IFN-induced necroptosis in MEFs (McComb et al., 2014; Thapa et al., 2013), while ablation of TNFR1, RIG-I/MAVS, or MyD88/TRIF will be expected to abolish RIPK3 activation by, respectively, TNF-α, RLRs, and TLRs. In each case, RIPK3-dependent cell death (Fig. 2E) and formation of the RIPK3-RIPK1 complex (Fig. S3) were largely indistinguishable between wild-type MEFs and MEFs deficient in type I IFN, TNF-α, RLR or TLR signaling. These results indicate that IAV replication either induces RIPK3-mediated cell death by mechanism(s) distinct from known RIPK3-activating pathways, or, alternatively, triggers redundant combinations of these pathways to activate RIPK3.

IAV activates parallel pathways of necroptosis and apoptosis downstream of RIPK3

Recent evidence shows that RIPK3 activates not only MLKL-driven necrotic cell death but, under certain conditions (e.g., when its kinase activity is inhibited or its conformation altered) caspase-dependent apoptosis as well (Mandal et al., 2014; Newton et al., 2014). To distinguish between apoptotic and necrotic cell death mechanisms activated by IAV downstream of RIPK3, we therefore examined the effects of selective RIPK1 and RIPK3 kinase inhibitors, as well as of the pan-caspase blocker zVAD, on viability of wild-type MEFs after infection with PR8. RIPK1 kinase blockade with GSK’963, GSK’481 or Nec-1 did not have any discernible protective effect on viability of MEFs after infection with PR8 (Fig. 3A), an observation in line with the inability of these agents to prevent IAV-driven necrosome formation (Fig. 2D). Surprisingly, RIPK3 kinase inhibition with GSK’872 or GSK’843 also failed to prevent PR8-induced cell death, although each of these inhibitors blocked PR8-induced necrosome assembly (Fig. 2D) and was fully protective against TNF-α-induced necroptosis at the same doses (Fig. 3A). Similarly, zVAD by itself did not protect MEFs from PR8-induced cell deaths (Fig. 3A) at a dose that prevented apoptosis induced by the combination of TRAIL and cycloheximide (not shown). But remarkably, the combination of RIPK3 kinase inhibitors with zVAD conferred almost full protection against PR8-induced cell death in both MEFs (Fig. 3A) and LET1 AECs (Fig. 3B). In similar studies on the necroptosis-competent human HT-29 cell line, we again found that IAV-activated cell death was not singly prevented by either caspase- or RIPK3 blockade, but was significantly rescued by the combined inhibition of caspases and RIPK3 kinase activity (Fig. 3C). Thus, IAV-activated RIPK3-dependent cell-death mechanisms appear conserved between humans and mice.

Notably, RIPK1 inhibitors deployed under similar conditions were incapable of protection against PR8 in the presence of zVAD (Fig. 3A). Together with our results from the use of these inhibitors in the necrosome assembly experiments shown in Fig. 2, these findings implicate a dominant role for the kinase activity of RIPK3, but not RIPK1, in PR8-driven necrotic death. They also indicate that parallel, redundant pathways of apoptosis and kinase-dependent necroptosis are activated by IAV infection downstream of RIPK3. In agreement with these observations, kinetic analysis of cell death in IAV-infected wild-type MEFs demonstrated that neither a caspase inhibitor nor an inhibitor of RIPK3 kinase function were singly able to protect against cell death, but the combined inhibition of caspases and RIPK3 kinase activity was significantly protective (Fig. 3D).

IAV induced both MLKL phosphorylation and cleavage of caspase 8 in MEFs, only the first of which was inhibited by RIPK3 kinase blockade and only the second by zVAD (Fig. 3E). Both MLKL phosphorylation and cleavage of caspase 8 were only seen in cells harboring actively-replicating IAV, and not in cells without detectable replicating virus, indicating that both arms of IAV-activated RIPK3-dependent cell death are phenomena restricted to the infected cell, and not the result of bystander activity on surrounding, uninfected cells (Fig. S4).

MLKL mediates necroptosis while FADD and caspase 8 drive apoptosis upon IAV infection

As MLKL has emerged as the primary effector of RIPK3-activated necroptosis, and as PR8-induced the robust phosphorylation of MLKL, we next evaluated the role of this pseudokinase in IAV-triggered cell death. Upon infection with PR8, primary *mlkl*$^{-/-}$ MEFs, unlike *ripk3*$^{-/-}$ MEFs, were not any more resistant to cell death than their wild-type counterparts, and succumbed to this virus with kinetics and magnitude indistinguishable from controls. Strikingly, *mlkl*$^{-/-}$ MEFs were fully rescued from PR8-induced cell death by pretreatment with zVAD alone, without need for concurrent inhibition of the kinase activity of RIPK3 (Fig. 4A). Pretreatment of *mlkl*$^{-/-}$ MEFs with the caspase 8-specific inhibitor zIETD also provided significant protection against PR8, while RIPK3 kinase blockade by itself had no effect (Fig. 4A). As levels of key effector proteins, including RIPK1 and RIPK3, are comparable between *mlkl*$^{+/+}$ and *mlkl* $^{-/-}$ MEFs (Fig. S2), these results provide unambiguous evidence that IAV-activated death signaling bifurcates downstream of RIPK3 into MLKL-driven necroptosis (which requires the kinase activity of RIPK3) and caspase-mediated apoptosis (which does not). They also implicate caspase 8 as a dominant caspase in the RIPK3-regulated cell death axis that results in apoptosis. Of note, zIETD consistently afforded less protection against PR8 than zVAD did, even when replenished at 12 h, in agreement with our previous findings that zIETD is weaker than zVAD at preventing caspase 8-driven apoptosis (McStay et al., 2008) (Fig. S5A).

Given our observation that the apoptosis adaptor protein FADD is recruited to the IAV-activated necrosome, we next asked if FADD was involved in the IAV-activated apoptosis arm downstream of RIPK3. Accordingly, we infected *fadd*$^{-/-}$ MEFs with PR8 and monitored the viability of these cells in the presence or absence of zVAD and/or RIPK3 inhibitors. *Fadd*$^{-/-}$ MEFs were somewhat more resistant to IAV-induced cell death than wild-type MEFs, as we had observed previously (Balachandran et al., 2000). This resistance

may be attributable, at least in part, to the reduced basal levels of MLKL seen in *fadd*$^{-/-}$ MEFs (Fig. S3, see also Fig. 4B) and reported previously by Vaux and colleagues (Cook et al., 2014). As *fadd*$^{-/-}$ MEFs display heightened basal necrosome activity (Thapa et al., 2013), diminished MLKL levels may supply a survival advantage to these cells, allowing their continued propagation in culture. Nonetheless, the loss of viability of *fadd*$^{-/-}$ MEFs following PR8 infection was almost completely rescued by pretreatment of these cells with RIPK3 kinase inhibitors, but not with zVAD (Fig. 4A).

These results indicate that MLKL and FADD each drive parallel, independent pathways of, respectively, necroptosis and apoptosis downstream of RIPK3. They also suggest that combined ablation of both MLKL and FADD will be needed to afford protection from IAV-induced cell death that is comparable to what is observed when RIPK3 is absent. To test this idea, we generated mice homozygously null for both *mlkl* and *fadd*. As will be reported in detail elsewhere (CD and DRG, manuscript submitted), ablating *mlkl* rescues the embryonic lethality of *fadd*$^{-/-}$ mice, and *mlkl*$^{-/-}$*fadd*$^{-/-}$ double knock-out mice are born at normal Mendelian frequency, exhibit no overt developmental defects, and survive into adulthood. When we infected primary MEFs from *mlkl*$^{-/-}$*fadd*$^{-/-}$ double knock-out mice with IAV, we found them to be remarkably (>95%) resistant to virus-induced cell death. Indeed, MEFs from these mice were even more resistant to IAV-triggered cell death than MEFs from *ripk3*-deficient mice, surviving for over 60 h.p.i. at an m.o.i. of 5 (Fig. S5B), without any obvious defects in either IAV infectivity (not shown) or replication (Fig. S5C). Thus, MLKL- and FADD-dependent cell death axes together almost completely account for IAV-triggered cell death, both downstream of RIPK3 and, indeed, independent of this kinase (Figs. 1F and S6). In accordance with these conclusions, *mlkl*$^{-/-}$ MEFs showed no defect in caspase 8 activation upon IAV infection, but (expectedly) displayed no MLKL phosphorylation, while *fadd*$^{-/-}$ MEFs were completely deficient in their capacity to activate caspase 8 after infection with IAV, but continue to support phosphorylation of MLKL (Fig. 4B). Only *mlkl*$^{-/-}$*fadd*$^{-/-}$ double knock-out MEFs, like *ripk3*$^{-/-}$ MEFs, were deficient in their ability to activate either pathway (Fig. 4B). Notably, both RIPK3-dependent ‘early apoptosis’ and RIPK3-independent ‘late apoptosis’ proceed normally on a background of MLKL deficiency, demonstrating the parallel nature of apoptosis and necroptosis pathways activated by IAV (Fig, S5D).

Of interest, *mlkl*$^{-/-}$*fadd*$^{-/-}$ double knock-out MEFs displayed altered mobility of RIPK1 and RIPK3 by SDS-PAGE, when compared to wild-type MEFs (Fig. S2). Pre-incubation of *mlkl*$^{-/-}$*fadd*$^{-/-}$ double knock-out MEFs with RIPK1 or RIPK3 kinase inhibitors demonstrate that, at least in the case of RIPK3, the slower-migrating band represents an auto-phosphorylated version of this kinase (not shown), suggesting unanticipated roles for FADD and MLKL in homeostatic control of basal RIPK1/3 expression and activity.

Role of RIPK1 in IAV-activated RIPK3-dependent cell death pathways

Although RIPK1 is robustly recruited to - and phosphorylated by - RIPK3 upon IAV infection, its role as a kinase in the execution of necroptosis following IAV infection appears unnecessary (Fig. 3A). As RIPK1 can function as an apoptosis adaptor downstream of RIPK3 (Cook et al., 2014; Mandal et al., 2014), we therefore sought to parse the roles of this

protein in RIPK3-activated cell death upon IAV infection. To this end, we infected *ripk1*$^{-/-}$ MEFs with PR8 and examined the viability of these cells in the presence or absence of zVAD or the RIPK3 inhibitors GSK'843 and GSK'872. *Ripk1*$^{-/-}$ MEFs, unlike *ripk3*$^{-/-}$ MEFs, displayed no significant resistance to PR8, and succumbed to this virus with kinetics indistinguishable from wild-type MEFs (Fig. 5A). *Ripk1*$^{-/-}$ MEFs, however, were almost-fully protected from PR8-induced cell death by pre-treatment with RIPK3 kinase inhibitors (but not with zVAD), demonstrating that, like FADD, RIPK1 was essential for the apoptosis axis downstream of RIPK3. Remarkably, MEFs from two distinct RIPK1 kinase-dead knock-in mice *[ripk1*$^{k45a/k45a}$ (Berger et al., 2014) and *ripk1*$^{d138n/d138n}$ (Polykratis et al., 2014)] phenocopied wild-type MEFs in their cell death responses to IAV, demonstrating that the kinase activity of RIPK1 was not required for activating apoptosis after infection (Fig. 5A). Expectedly, *ripk1*$^{-/-}$ MEFs, as well as MEFs from RIPK1 kinase-dead knock-in mice, were resistant to TNF-α-induced necroptosis, where RIPK1 functions as a kinase to activate RIPK3 and drive necrotic cell death (Cho et al., 2009; Vandenabeele et al., 2010) (Fig. 5B). In accordance with these findings, IAV-induced phosphorylation of MLKL was intact in *ripk1*$^{-/-}$ MEFs and in MEFs from RIPK1 kinase-dead knock-in (*ripk1*$^{d138n/d138n}$) mice, while caspase 8 activity was selectively lost in *ripk1*$^{-/-}$ MEFs, and not in MEFs expressing kinase-dead RIPK1 (Fig. 5C). Subsequent immunoprecipitation experiments revealed that PR8-induced association of FADD with RIPK3 was dependent on RIPK1 (Fig. 5D), placing RIPK1 upstream of FADD and functionally implicating RIPK1 as a kinase-independent adaptor protein that links RIPK3 to FADD and caspase 8 during IAV-activated apoptosis.

MLKL- and FADD-driven arms of RIPK3-mediated cell death functionally overlap in protecting against lethal IAV infection *in vivo*

To examine the effect of RIPK3 deficiency on the host response to respiratory infection with IAV, we inoculated cohorts of *ripk3*$^{-/-}$ mice, alongside their age-and sex-matched wild-type controls, with PR8 and monitored their survival over a time course of 18 days. We found that ~25% of wild-type (*ripk3*$^{+/+}$) controls succumbed to PR8 by 15 d.p.i.; mice surviving past this time point recovered fully. Loss of *ripk3* resulted in significantly increased lethality ($p < 0.05$), with 60% of *ripk3*$^{-/-}$ mice succumbing to PR8 in the same time frame (Fig. 6A). When we examined progeny virion production in infected mice, we found no notable difference in virus output on day 3 p.i., but observed ~10-fold more virus in the lungs of *ripk3*$^{-/-}$ mice than those of control animals on day 9 p.i. (Fig. 6C).

To identify the relative contributions of MLKL-mediated necroptosis versus FADD-induced apoptosis downstream of RIPK3 in control of IAV *in vivo*, we next infected wild-type (*mlkl*$^{+/+}$), *mlkl*$^{-/-}$, and *mlkl*$^{-/-}$*fadd*$^{-/-}$ double knock-out mice with PR8 and monitored their survival over 18 days. *Fadd*$^{-/-}$ mice die *in utero* (Yeh et al., 1998), precluding their use from these experiments. Interestingly, *mlkl*$^{-/-}$ mice were not any more susceptible to IAV than their wild-type counterparts and the majority (~75%) of these mice survived this dose of PR8 to recover fully from infection (Fig. 6B). In agreement with these findings, *mlkl*$^{-/-}$ mice did not differ significantly from wild-type animals in lung progeny virion output either early (day 3) or late (day 9) post-infection (Fig. 6C). Mice doubly-deficient in MLKL and FADD, however, were extremely susceptible to IAV-induced lethality, with none surviving past day 12 p.i (Fig. 6B). These mice were also severely compromised in their capacity to

limit IAV replication; although virus titers from infected *mlkl*$^{-/-}$*fadd*$^{-/-}$ lungs were similar to those seen in wild-type animals early in infection, these titers did not drop during the resolution phase (day 9) of infection, remaining ~20–100-fold higher than levels observed in controls (Fig. 6C).

To explore the basis for the elevated mortality of *ripk3*$^{-/-}$ mice, we performed histological analyses of lungs 6 d.p.i. We stained lung sections with anti-IAV antibody to determine the extent of infection and with hematoxylin/eosin to assess lesion severity. Compared to *ripk3*$^{+/+}$ littermate controls, *ripk3*$^{-/-}$ lungs exhibited a significant increase in virus spread within the infected lung (Fig. 6D), consistent with our previous observations that *ripk3*$^{-/-}$ mice fail to effectively control IAV progeny virion production (Fig. 6C). We also noted substantial pulmonary edema and an increase in alveolar fibrin deposition in *ripk3*$^{-/-}$ lungs, indicative of severe damage to the capillaries and alveoli in these animals (Fig. 6E). Deposition of fibrin around the alveoli of infected *ripk3*$^{-/-}$ lungs is likely indicative of a 'cytokine storm'-driven inflammatory response to increased virus spread within lung tissue.

As RIPK3 can also drive immune responses (Pasparakis and Vandenabeele, 2015), we examined the effect of RIPK3 loss on the recruitment of T cells to the infected lung. Lungs from *ripk3*$^{-/-}$ displayed a markedly reduced infiltration of CD3^{+} cells, compared to *ripk3*$^{+/+}$ controls, 6 d.p.i. (Fig. 6F). To examine this effect in greater detail, we first measured the abundance of IAV-specific CD8^{+} T cells in bronchioalveolar lavage (BAL) fluid 9 d.p.i., and found that IAV-specific CD8^{+} T cell numbers were significantly diminished in *ripk3*$^{-/-}$ mice (Fig. 6G, left). Moreover, responding *ripk3*$^{-/-}$ CD8^{+} T cells appeared less capable of mounting an efficient effector response, as evidenced by the lower frequencies of polyfunctional (IFN-γ^{+}TNF-α^{+}) CD8^{+} T cells in BAL fluid of *ripk3*$^{-/-}$ mice, compared to *ripk3*$^{+/+}$ controls. (Fig. 6G, right). Collectively, these findings denote that loss of RIPK3 results not only in increased IAV spread within the infected lung, but also in diminished antiviral CD8^{+} T cell responses to the infection.

Discussion

In this study, we demonstrate that RIPK3 activates parallel pathways of necroptotic and apoptotic death following IAV infection of fibroblasts and lung epithelial cells (Fig. S6). Activation of RIPK3 requires virus replication, suggesting that PAMPs produced during the virus life-cycle are directly recognized by an upstream sensor(s) that then stimulates RIPK3. Alternatively, such PAMPs may activate RIPK3 more indirectly, for example through the autocrine activity of virus-induced pro-necrotic cytokines such as type I IFNs or TNF-α. Our data do not support an essential role for either IFNs, TNF-α, the RLR-MAVS axis, or TLR signaling, in mediating RIPK3 activation upon IAV infection. Zhou and colleagues similarly found that RIPK1/RIPK3-driven activation of the NLRP3 inflammasome by RNA viruses also proceeded independently of known RNA-sensing antiviral receptors (Wang et al., 2014a), indicating that either two or more of these pathways are concurrently required to activate RIPK3, or that an as-yet unknown sensor(s) recognizes IAV to stimulate this kinase. An intriguing third possibility is that an IAV-encoded protein may directly activate RIPK3, as was recently shown to occur in the context of an acute HSV-1 infection of murine cells,

where the RHIM-containing virus-encoded protein ICP6 activated murine RIPK3 by directly interacting with a component of a viral genome (Huang et al., 2015; Wang et al., 2014b).

Once activated, what dictates whether RIPK3 triggers necrosis or apoptosis in infected cells? This decision may be a stochastic one, determined by local availability of MLKL versus RIPK1, caspase 8 or FADD in the infected cell, or of other molecular determinants downstream of these proteins. IAV can trigger necroptosis in cells in which caspase 8 is not only present, but also readily activated during infection with kinetics that parallel MLKL activation. The mechanism(s) by which IAV activates RIPK3-mediated cell death thus appears distinct from other DNA viruses, where virus-encoded inhibitors are required to suppress caspase 8 activity for necroptosis to proceed (Mocarski et al., 2014). The fact that IAV activates MLKL without need for concurrent caspase 8 suppression lends support to the 'stochastic availability' model, in which both apoptosis and necroptosis can be equivalently deployed downstream of RIPK3, but cell-type specific differences in abundance (Cook et al., 2014) or localization of effector proteins determine if the infected cell undergoes apoptosis, necroptosis, or both, following RIPK3 activation. In some cases, such as in a small population of club cells shown by tenOever and colleagues as capable of surviving an influenza A infection *in vivo* (Heaton et al., 2014), it is possible that none of these pathways are activated.

Alternatively, a more-active molecular switch mechanism may exist that alters the cell fate decision between kinase-dependent necroptosis and kinase-independent apoptosis downstream of RIPK3, much as de-ubiquitylation of RIPK1 has been shown to switch this protein from kinase-independent activator of survival signaling to kinase-dependent cell death inducer (Weinlich and Green, 2014). Both RIPK3 and MLKL are ubiquitylated upon TLR stimulation, and their ubiquitylation in this context is modulated by the IAP family of E3 ligases (Lawlor et al., 2015). As cIAP1 loss greatly exacerbates RIPK3-driven lung pathology during an acute IAV infection (Rodrigue-Gervais et al., 2014), it is very likely that ubiquitylation, particularly by the IAPs, controls the activity of RIPK3 and other regulators to determine cell fate responses to IAV. The 'stochastic availability' and 'molecular switch' models are not necessarily mutually-exclusive in the context of an active infection *in vivo*; each may operate in settings that are dictated by temporal and cell type-specific cues.

RIPK3-driven cell death may aid in virus clearance by at least two mechanisms: (1) by preventing infected cells from becoming 'factories' for virus replication, and (2) by promoting activation of adaptive immunity via release of immunogenic danger-associated molecular patterns (DAMPs) from dead or dying cells. Our immunophenotyping assessments of infected lung tissue revealed significantly diminished T cell recruitment and anti-IAV adaptive immune responses in susceptible *ripk3*$^{-/-}$ mice, despite notably higher progeny virion output in these animals, suggesting that inhibition of virus replication by both active lysis of the infected cell, and by secondary stimulation of the adaptive immune response, collaboratively underlie the capacity of RIPK3 to control IAV. Notably, the NLRP3 inflammasome is required for protection against IAV (Allen et al., 2009; Ichinohe et al., 2009; Thomas et al., 2009), so RIPK3-driven activation of the NLRP3 inflammasome (Wang et al., 2014a) may co-operate with cell death induction in mediating virus clearance and promoting the healing of infected lung tissue.

Although RIPK3-mediated cell death and inflammasome pathways are clearly essential to effective clearance of an IAV infection, it is noteworthy that mice lacking both FADD and MLKL are more-severely impaired in their ability to control IAV, and also significantly more susceptible to this virus, that RIPK3-deficient mice. Similarly, cells lacking both FADD and MLKL, or RIPK3 knock-out MEFs additionally deficient in FADD or caspase 8, are considerably more resistant to IAV-induced cell death than MEFs lacking only RIPK3. These observations demonstrate that RIPK3-independent apoptosis pathway(s) reliant on FADD and caspase 8 are also engaged by IAV and function in tandem with RIPK3-driven cell death and inflammasome activation in eliminating the infected cell to limit virus spread.

Experimental Procedures

Mice and cells

Ripk3$^{-/-}$, *ripk3*$^{-/-}$*casp8*$^{-/-}$, *fadd*$^{-/-}$, *ripk3*$^{-/-}$*fadd*$^{-/-}$, *mlkl*$^{-/-}$, *ripk3*$^{-/-}$*mlkl*$^{-/-}$, *mlkl*$^{-/-}$*fadd*$^{-/-}$, *ripk1*$^{-/-}$, *ripk1*$^{k45/a/k45a}$, *ripk1*$^{d138n/d138n}$, *ifnar1*$^{-/-}$, *stat1*$^{-/-}$, *eif2ak2*$^{-/-}$, *mavs*$^{-/-}$, and *tnfr1*$^{-/-}$ MEFs were generated in-house from E14.5 embryos and used within five passages in experiments. Early passage *ddx58*$^{-/-}$ and *myd88−/−trif-* MEFs were purchased from Oriental BioService Inc. (Osaka, Japan). LET1 cells have been described before (Rosenberger et al., 2014). HT-29 cells were obtained from the American Type Culture Collection (Manassas, VA).

Reagents

Biological and chemical reagents were from the following sources: Necrostatin 1 (BioVision), Nucleozin (Sigma), Q-VD-OPh (Apexbio), zIETD.fmk (Calbiochem), zVAD.fmk (Bachem), mIFN-β (PBL), murine and human TNF-α (R&D systems), mTRAIL (R&D systems), SMAC mimetic LCL161 (Chemietek). Inhibitors of RIPK1 [GSK'481, GSK'963 (Harris et al., 2013)] and RIPK3 [GSK'840, GSK'872, GSK'843 (Mandal et al., 2014)] from GlaxoSmithKline have been described before. Antibodies for immunoblot analysis of β-actin (Sigma), caspase 8 (Cell Signaling), cleaved caspase 8 (Cell Signaling), FADD (Millipore), IAV NP (BioRad), IAV NS1 (Santa Cruz), MLKL (Abgent or Millipore), p-MLKL (Abcam), RIPK1 (BD Transduction Labs), RIPK3 (ProSci or Santa Cruz), were obtained from the indicated commercial sources. Neutralizing antibodies to mTNF-α (Cell Signaling) and mTRAIL-R2 (R&D systems) were obtained from the indicated sources. Antiserum to PR8 was produced in-house at the Fox Chase Cancer Center. For detection of IAV and CD3 in paraffin-embedded tissue, anti-IAV antibodies (US Biologicals) and anti-CD3 antibodies (Santa Cruz) were used. For FACS, antibodies to CD8α (clone 53-6.7), anti-CD16/CD32 (clone 2.4G2), anti-TNF-α (clone MP6-XT22), anti-IFN-γ (clone XMG1.2), and anti-CD28 were obtained from BD PharMingen.

Viruses

IAV strains PR8 and A/HKx31 were generated by reverse genetics as previously described (Hoffmann et al., 2002). All IAV and IBV strains were propagated by allantoic inoculation of embryonated hen's eggs with diluted ($1:10^6$) seed virus. Virus titers were determined as 50% egg infectious dose (EID_{50}) and by plaque assay on Madin-Darby Canine Kidney

(MDCK) cells. Recombinant PR8-GFP virus has been described previously (Manicassamy et al., 2010).

Virus infection and titration

Mice were anesthetized with Avertin (2,2,2-tribromoethanol) or isoflurane and infected intranasally with virus inoculum diluted in endotoxin-free phosphate-buffered saline. Mice were either monitored for survival and weight loss over a period of 18 days or sacrificed at defined time points for analysis of histology and virus replication. Mice losing >35% bodyweight were considered moribund and euthanized by CO_2 asphyxiation. To determine progeny virus production in infected mice, lung homogenates were titered by plaque assay on MDCK cells, as described previously (Thomas et al., 2009). For cell culture experiments, near-confluent monolayers of cells were infected with virus in serum-free DMEM for 1 h, with occasional gentle rocking, in a humidified tissue culture incubator maintained at 37°C and 5% CO_2. Following infection, the inoculum was removed and replaced with growth medium. In conditions involving small-molecule inhibitors, cells were pre-incubated for 1 h with inhibitors before infection; after removal of inoculum and washing, inhibitors were added back to the medium. Titration of virus from supernatants of infected LET1 cells was determined by a chicken red blood cell-based hemagglutination assay, as described previously (Po et al., 2002). Cell viability was determined by Trypan Blue exclusion or on an Incucyte Kinetic Live Cell Imaging System (Essen Bioscience).

Supplementary Material

Refer to Web version on PubMed Central for supplementary material.

Acknowledgments

We are grateful to Vishva Dixit, Adolfo Garcia-Sastre, Scott Hensley, Ganes Sen and Luis Sigal viruses, cells, and mice. This work was supported by NIAID contract HHSN272201400006C (St. Jude Center of Excellence for Influenza Research and Surveillance) to PGT, NIH grant AI109472 to CBL, NIH grants AI44828 and CA169291 to DRG, and NIH grants CA168621, CA190542 and AI113469 to SB. Additional funds were provided by the F.M. Kirby Foundation, and via NIH Cancer Center Support Grant P30CA006927 to SB.

References

Allen IC, Scull MA, Moore CB, Holl EK, McElvania-TeKippe E, Taxman DJ, Guthrie EH, Pickles RJ, Ting JP. The NLRP3 inflammasome mediates in vivo innate immunity to influenza A virus through recognition of viral RNA. Immunity. 2009; 30:556–565. [PubMed: 19362020]

Amorim MJ, Read EK, Dalton RM, Medcalf L, Digard P. Nuclear export of influenza A virus mRNAs requires ongoing RNA polymerase II activity. Traffic. 2007; 8:1–11. [PubMed: 17132145]

Balachandran S, Roberts PC, Kipperman T, Bhalla KN, Compans RW, Archer DR, Barber GN. Alpha/beta interferons potentiate virus-induced apoptosis through activation of the FADD/Caspase-8 death signaling pathway. J. Virol. 2000; 74:1513–1523. [PubMed: 10627563]

Berger SB, Harris P, Nagilla R, Kasparcova V, Hoffman S, Swift B, Dare L, Schaeffer M, Capriotti C, Ouellette M, et al. Characterization of GSK′963: a structurally distinct, potent and selective inhibitor of RIP 1 kinase. Cell Death Discovery. 2015; 1:15009. [PubMed: 27551444]

Berger SB, Kasparcova V, Hoffman S, Swift B, Dare L, Schaeffer M, Capriotti C, Cook M, Finger J, Hughes-Earle A, et al. Cutting Edge: RIP1 kinase activity is dispensable for normal development but is a key regulator of inflammation in SHARPIN-deficient mice. J Immunol. 2014; 192:5476–5480. [PubMed: 24821972]

Brandes M, Klauschen F, Kuchen S, Germain RN. A systems analysis identifies a feedforward inflammatory circuit leading to lethal influenza infection. Cell. 2013; 154:197–212. [PubMed: 23827683]

Chan FK, Luz NF, Moriwaki K. Programmed necrosis in the cross talk of cell death and inflammation. Annu Rev Immunol. 2015; 33:79–106. [PubMed: 25493335]

Cho YS, Challa S, Moquin D, Genga R, Ray TD, Guildford M, Chan FK. Phosphorylation-driven assembly of the RIP1-RIP3 complex regulates programmed necrosis and virus-induced inflammation. Cell. 2009; 137:1112–1123. [PubMed: 19524513]

Cook WD, Moujalled DM, Ralph TJ, Lock P, Young SN, Murphy JM, Vaux DL. RIPK1- and RIPK3-induced cell death mode is determined by target availability. Cell Death Differ. 2014; 21:1600–1612. [PubMed: 24902899]

Degterev A, Hitomi J, Germscheid M, Ch'en IL, Korkina O, Teng X, Abbott D, Cuny GD, Yuan C, Wagner G, et al. Identification of RIP1 kinase as a specific cellular target of necrostatins. Nat Chem Biol. 2008; 4:313–321. [PubMed: 18408713]

Harris PA, Bandyopadhyay D, Berger SB, Campobasso N, Capriotti CA, Cox JA, Dare L, Finger JN, Hoffman SJ, Kahler KM, et al. Discovery of Small Molecule RIP1 Kinase Inhibitors for the Treatment of Pathologies Associated with Necroptosis. ACS Med Chem Lett. 2013; 4:1238–1243. [PubMed: 24900635]

Harris PA, King BW, Bandyopadhyay D, Berger SB, Campobasso N, Capriotti CA, Cox JA, Dare L, Dong X, Finger JN, et al. DNA-Encoded Library Screening Identifies Benzo[b][1,4]oxazepin-4-ones as Highly Potent and Monoselective Receptor Interacting Protein 1 Kinase Inhibitors. J Med Chem. 2016; 59:2163–2178. [PubMed: 26854747]

Heaton NS, Langlois RA, Sachs D, Lim JK, Palese P, tenOever BR. Long-term survival of influenza virus infected club cells drives immunopathology. J Exp Med. 2014; 211:1707–1714. [PubMed: 25135297]

Hoffmann E, Krauss S, Perez D, Webby R, Webster RG. Eight-plasmid system for rapid generation of influenza virus vaccines. Vaccine. 2002; 20:3165–3170. [PubMed: 12163268]

Huang Z, Wu SQ, Liang Y, Zhou X, Chen W, Li L, Wu J, Zhuang Q, Chen C, Li J, et al. RIP1/RIP3 binding to HSV-1 ICP6 initiates necroptosis to restrict virus propagation in mice. Cell Host Microbe. 2015; 17:229–242. [PubMed: 25674982]

Ichinohe T, Lee HK, Ogura Y, Flavell R, Iwasaki A. Inflammasome recognition of influenza virus is essential for adaptive immune responses. J Exp Med. 2009; 206:79–87. [PubMed: 19139171]

Kao RY, Yang D, Lau LS, Tsui WH, Hu L, Dai J, Chan MP, Chan CM, Wang P, Zheng BJ, et al. Identification of influenza A nucleoprotein as an antiviral target. Nat Biotechnol. 2010; 28:600–605. [PubMed: 20512121]

Kash JC, Tumpey TM, Proll SC, Carter V, Perwitasari O, Thomas MJ, Basler CF, Palese P, Taubenberger JK, Garcia-Sastre A, et al. Genomic analysis of increased host immune and cell death responses induced by 1918 influenza virus. Nature. 2006; 443:578–581. [PubMed: 17006449]

Lawlor KE, Khan N, Mildenhall A, Gerlic M, Croker BA, D'Cruz AA, Hall C, Kaur Spall S, Anderton H, Masters SL, et al. RIPK3 promotes cell death and NLRP3 inflammasome activation in the absence of MLKL. Nat Commun. 2015; 6:6282. [PubMed: 25693118]

Mandal P, Berger SB, Pillay S, Moriwaki K, Huang C, Guo H, Lich JD, Finger J, Kasparcova V, Votta B, et al. RIP3 induces apoptosis independent of pronecrotic kinase activity. Mol Cell. 2014; 56:481–495. [PubMed: 25459880]

Manicassamy B, Manicassamy S, Belicha-Villanueva A, Pisanelli G, Pulendran B, Garcia-Sastre A. Analysis of in vivo dynamics of influenza virus infection in mice using a GFP reporter virus. Proc Natl Acad Sci U S A. 2010; 107:11531–11536. [PubMed: 20534532]

McComb S, Cessford E, Alturki NA, Joseph J, Shutinoski B, Startek JB, Gamero AM, Mossman KL, Sad S. Type-I interferon signaling through ISGF3 complex is required for sustained Rip3 activation and necroptosis in macrophages. Proc Natl Acad Sci U S A. 2014; 111:E3206–E3213. [PubMed: 25049377]

McStay GP, Salvesen GS, Green DR. Overlapping cleavage motif selectivity of caspases: implications for analysis of apoptotic pathways. Cell Death Differ. 2008; 15:322–331. [PubMed: 17975551]

Mocarski ES, Kaiser WJ, Livingston-Rosanoff D, Upton JW, Daley-Bauer LP. True grit: programmed necrosis in antiviral host defense, inflammation, and immunogenicity. J Immunol. 2014; 192:2019–2026. [PubMed: 24563506]

Newton K, Dugger DL, Wickliffe KE, Kapoor N, de Almagro MC, Vucic D, Komuves L, Ferrando RE, French DM, Webster J, et al. Activity of protein kinase RIPK3 determines whether cells die by necroptosis or apoptosis. Science. 2014; 343:1357–1360. [PubMed: 24557836]

Pasparakis M, Vandenabeele P. Necroptosis and its role in inflammation. Nature. 2015; 517:311–320. [PubMed: 25592536]

Po JL, Gardner EM, Anaraki F, Katsikis PD, Murasko DM. Age-associated decrease in virus-specific CD8+ T lymphocytes during primary influenza infection. Mechanisms of ageing and development. 2002; 123:1167–1181. [PubMed: 12044966]

Polykratis A, Hermance N, Zelic M, Roderick J, Kim C, Van TM, Lee TH, Chan FK, Pasparakis M, Kelliher MA. Cutting edge: RIPK1 Kinase inactive mice are viable and protected from TNF-induced necroptosis in vivo. J Immunol. 2014; 193:1539–1543. [PubMed: 25015821]

Rodrigue-Gervais IG, Labbe K, Dagenais M, Dupaul-Chicoine J, Champagne C, Morizot A, Skeldon A, Brincks EL, Vidal SM, Griffith TS, et al. Cellular inhibitor of apoptosis protein cIAP2 protects against pulmonary tissue necrosis during influenza virus infection to promote host survival. Cell Host Microbe. 2014; 15:23–35. [PubMed: 24439895]

Rosenberger CM, Podyminogin RL, Askovich PS, Navarro G, Kaiser SM, Sanders CJ, McClaren JL, Tam VC, Dash P, Noonan JG, et al. Characterization of innate responses to influenza virus infection in a novel lung type I epithelial cell model. J Gen Virol. 2014; 95:350–362. [PubMed: 24243730]

Sanders CJ, Doherty PC, Thomas PG. Respiratory epithelial cells in innate immunity to influenza virus infection. Cell Tissue Res. 2011; 343:13–21. [PubMed: 20848130]

Sridharan H, Upton JW. Programmed necrosis in microbial pathogenesis. Trends Microbiol. 2014; 22:199–207. [PubMed: 24565922]

Thapa RJ, Nogusa S, Chen P, Maki JL, Lerro A, Andrake M, Rall GF, Degterev A, Balachandran S. Interferon-induced RIP1/RIP3-mediated necrosis requires PKR and is licensed by FADD and caspases. Proc Natl Acad Sci U S A. 2013; 110:E3109–E3118. [PubMed: 23898178]

Thomas PG, Dash P, Aldridge JR Jr, Ellebedy AH, Reynolds C, Funk AJ, Martin WJ, Lamkanfi M, Webby RJ, Boyd KL, et al. The intracellular sensor NLRP3 mediates key innate and healing responses to influenza A virus via the regulation of caspase-1. Immunity. 2009; 30:566–575. [PubMed: 19362023]

Vandenabeele P, Declercq W, Van Herreweghe F, Vanden Berghe T. The role of the kinases RIP1 and RIP3 in TNF-induced necrosis. Sci Signal. 2010; 3 re4.

Vaux DL, Haecker G, Strasser A. An evolutionary perspective on apoptosis. Cell. 1994; 76:777–779. [PubMed: 8124715]

Wang X, Jiang W, Yan Y, Gong T, Han J, Tian Z, Zhou R. RNA viruses promote activation of the NLRP3 inflammasome through a RIP1-RIP3-DRP1 signaling pathway. Nat Immunol. 2014a; 15:1126–1133. [PubMed: 25326752]

Wang X, Li Y, Liu S, Yu X, Li L, Shi C, He W, Li J, Xu L, Hu Z, et al. Direct activation of RIP3/MLKL-dependent necrosis by herpes simplex virus 1 (HSV-1) protein ICP6 triggers host antiviral defense. Proc Natl Acad Sci U S A. 2014b; 111:15438–15443. [PubMed: 25316792]

Weinlich R, Green DR. The two faces of receptor interacting protein kinase-1. Mol Cell. 2014; 56:469–480. [PubMed: 25459879]

Yatim N, Albert ML. Dying to replicate: the orchestration of the viral life cycle, cell death pathways, and immunity. Immunity. 2011; 35:478–490. [PubMed: 22035840]

Yeh WC, Pompa JL, McCurrach ME, Shu HB, Elia AJ, Shahinian A, Ng M, Wakeham A, Khoo W, Mitchell K, et al. FADD: essential for embryo development and signaling from some, but not all, inducers of apoptosis. Science. 1998; 279:1954–1958. [PubMed: 9506948]

Highlights

- RIPK3-deficient cells are resistant to IAV-induced death.
- RIPK3 activates both necroptosis and apoptosis upon IAV infection.
- RIPK3-mediated necroptosis requires MLKL, while apoptosis necessitates FADD.
- RIPK3-activated apoptosis compensates for loss of necroptosis *in vivo*

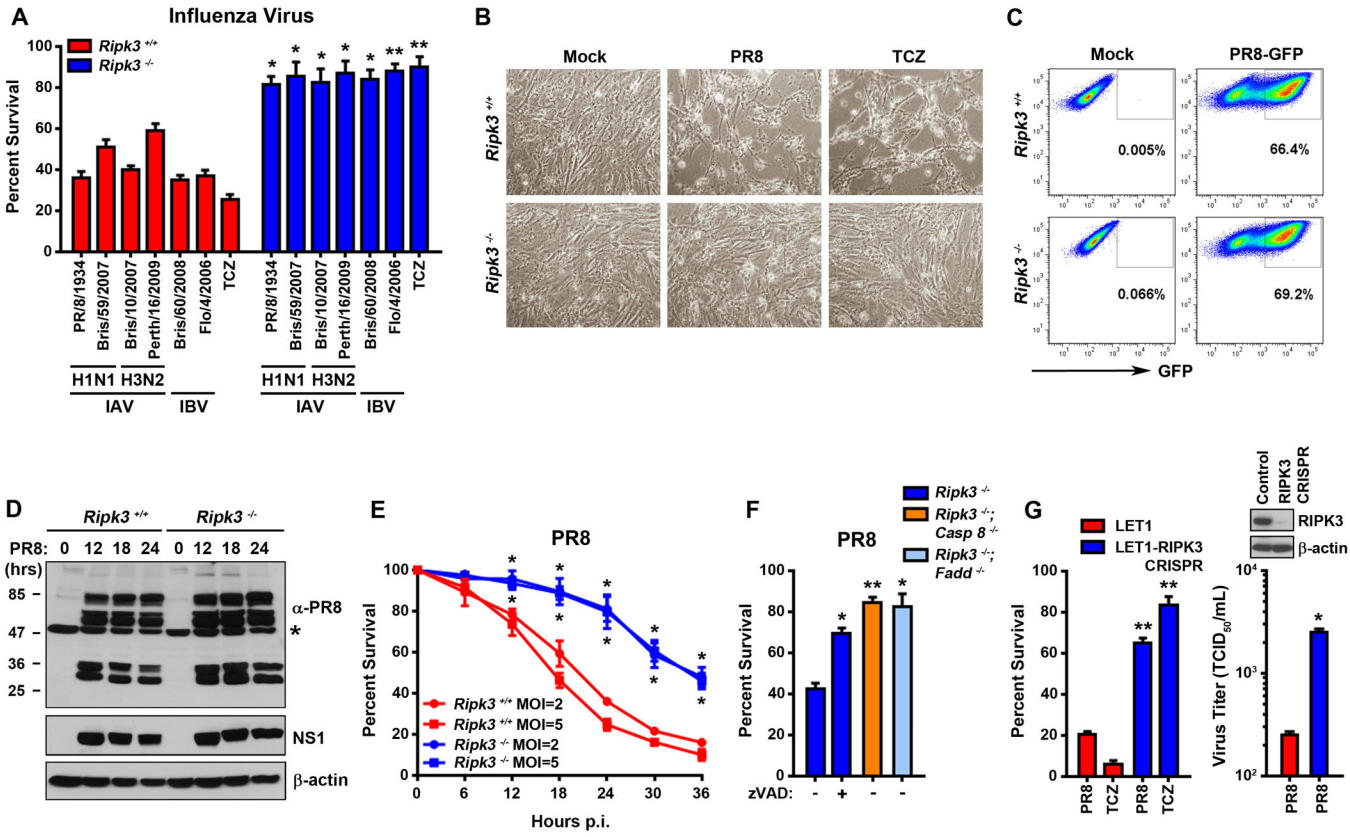

Figure 1. RIPK3 is required for IAV-induced lysis of MEFs and alveolar epithelial cells

(A) *Ripk3*$^{+/+}$ and *ripk3*$^{-/-}$ MEFs were infected with the indicated strains of influenza virus at m.o.i.=2 or treated with TNF-α (50ng/ml) in the presence of cycloheximide (250ng/ml) and zVAD (50μM) and cell viability was determined at 24 h.p.i. **(B)** Photomicrographs of *ripk3*$^{+/+}$ and *ripk3*$^{-/-}$ MEFs infected with PR8 or treated with TCZ for 24 h. **(C)** FACS analysis of *ripk3*$^{+/+}$ and *ripk3*$^{-/-}$ *MEFs* infected with PR8-GFP (m.o.i.=2). The y-axis shows side scatter. **(D)** *Ripk3*$^{+/+}$ and *ripk3*$^{-/-}$ MEFs infected with PR8 were examined for virus replication by immunoblotting with antiserum raised against PR8 or a monoclonal antibody to NS1. A non-specific band detected in uninfected lysates by the anti-PR8 antiserum is indicated with an asterisk (*). Molecular weights (in kDa) are shown to the left. **(E)** Kinetics of cell death after PR8 infection of *ripk3*$^{+/+}$ and *ripk3*$^{-/-}$ MEFs at the indicated m.o.i.s. **(F)** *Ripk3*$^{-/-}$ (in the presence or absence of 50μM zVAD), *ripk3*$^{-/-}$*casp8*$^{-/-}$, or *ripk3*$^{-/-}$*fadd*$^{-/-}$ MEFs were infected with PR8 and cell viability was determined 36 h.p.i. **(G)** Parental LET1 lung epithelial cells, or LET1 cells in which RIPK3 expression was ablated by CRISPR/Cas9 targeting of the sequence 5'-TGAGAACGTTCTGCTCCTGC-3' in the murine *ripk3* gene, were infected with PR8 and viability (left) or progeny virion output (right) was determined 12 h.p.i. *Inset:* Immunoblot showing RIPK3 levels in these cells, with β-actin included as a loading control. Error bars represent mean +/− S.D. * p <0.05; ** p <0.005. See also Figs. S1, S2 and S6.

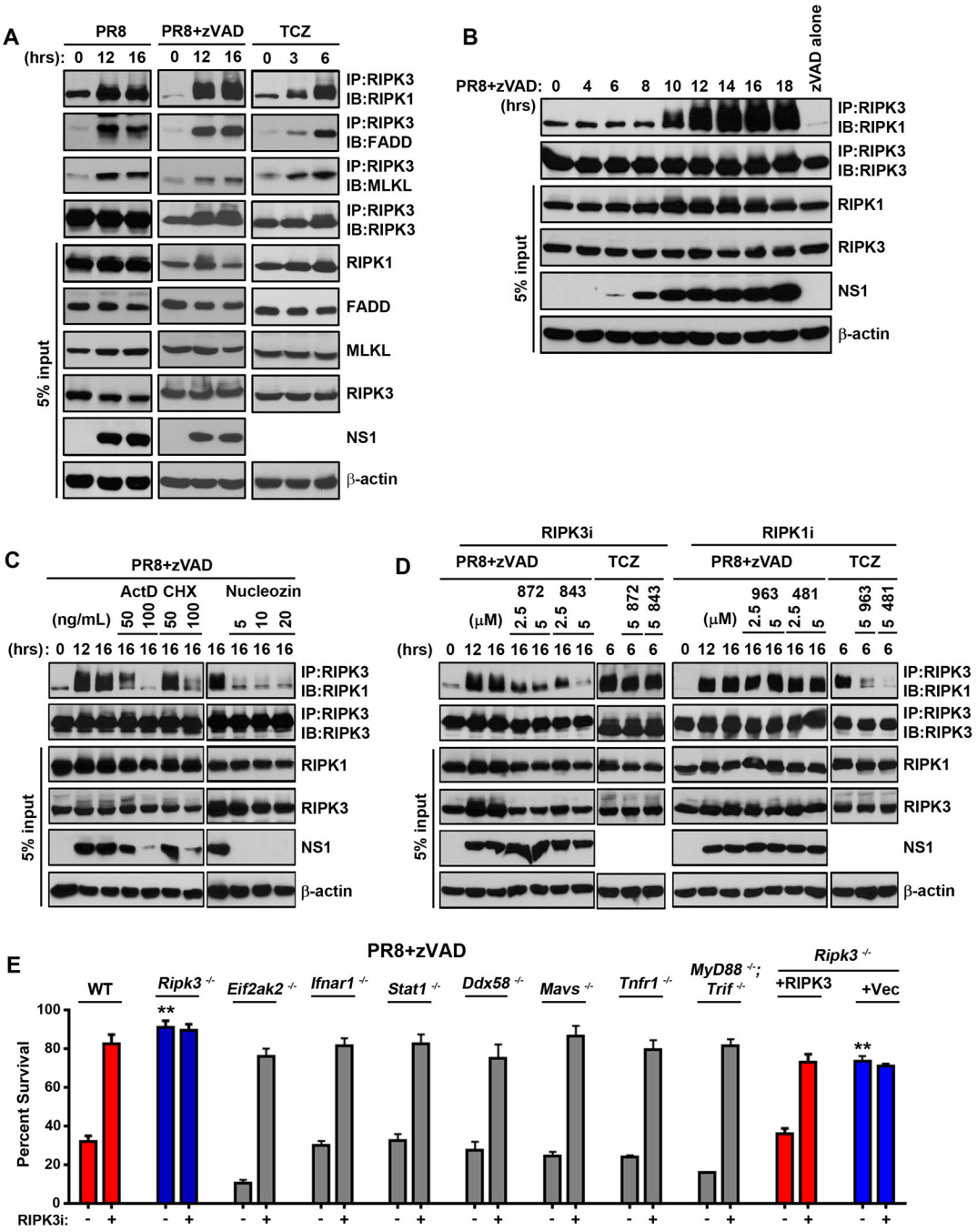

Figure 2. IAV activates formation of a RIPK3-containing necrosome complex

(A) Wild type MEFs were infected with PR8 (m.o.i.=2) in the presence or absence of zVAD (25μM), or treated with TCZ (right). Cells were lysed at the indicated time points, and anti-RIPK3 immunoprecipitates were examined for necrosome formation as described before (Thapa et al., 2013). IAV- or TCZ-activated RIPK3-RIPK1 necrosomes additionally contain FADD and MLKL. Whole-cell extract (5% input) was examined in parallel for RIPK1, RIPK3, FADD, MLKL, and IAV NS1 proteins. **(B)** Time course of RIPK1/RIPK3 necrosome formation demonstrates that necrosome assembly succeeds virus replication. **(C)**

RIPK3 immunoprecipitations performed on extracts from PR8-infected MEFs that were pre-treated with the indicated doses of Actinomycin D (ActD), cycloxehimide (CHX) or Nucleozin (Nuc), before infection indicates that the IAV-induced necrosome formation requires ongoing transcription, translation, and viral replication. **(D)** RIPK3 immunoprecipitations were performed on extracts from MEFs infected with PR8 or treated with TCZ in the presence or absence of the indicated doses of the RIPK3 kinase inhibitors GSK'872 or GSK'843 (left) or the RIPK1 kinase inhibitors GSK'963 or GSK'481 (right). **(E)** Primary early passage wild-type (WT) and the indicated knock-out MEFs were infected with PR8 in the presence of zVAD (50μM) with or without the RIPK3 inhibitor GSK'843 (5μM). As controls, *ripk3*$^{-/-}$ MEFs retrovirally reconstituted with full-length murine RIPK3, or with an empty vector, were used. Viability was determined 24 h.p.i. Error bars represent mean +/− S.D. ** p <0.005. See also Figs. S3 and S6.

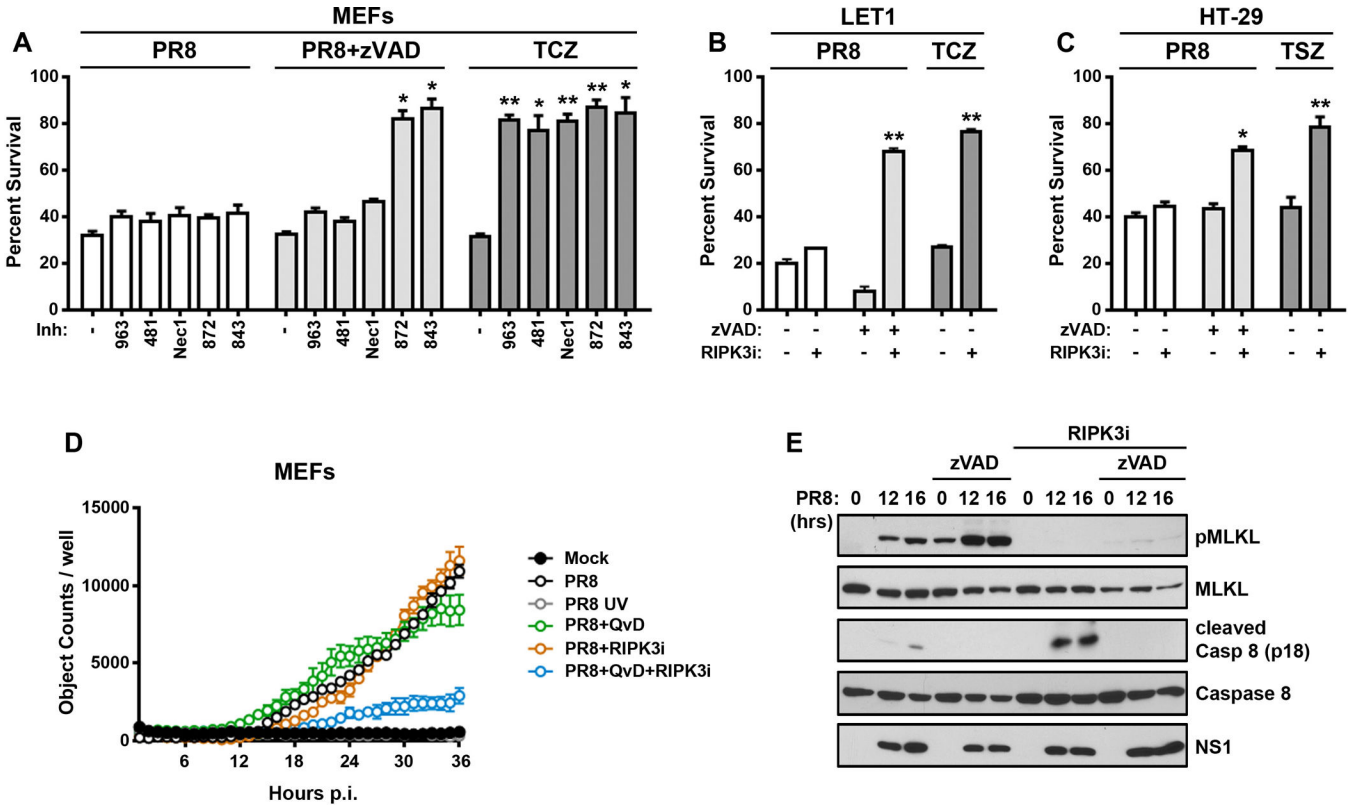

Figure 3. RIPK3 activates parallel pathways of necroptosis and apoptosis upon IAV infection

(A) *Ripk3*$^{+/+}$ MEFs were infected with PR8 (m.o.i.=2) in the presence or absence of zVAD (50μM), RIPK1 kinase inhibitors [GSK'963 (5μM), GSK'481 (5μM), and Nec-1 (50μM)], or RIPK3 kinase inhibitors [GSK'872 (5μM), and GSK'843 (5μM)] and cell viability was determined 24 h.p.i. TCZ-treated wild-type MEFs exposed to the same doses of RIPK1 or RIPK3 inhibitors were used as controls. **(B)** LET1 lung epithelial cells were infected with PR8 in the presence or absence of zVAD (50μM) or GSK'843 (5μM), and viability was determined 12 h.p.i. LET1 cells treated with TCZ were included as controls. **(C)** Human HT-29 cells were infected with PR8 (m.o.i.=5) in the presence or absence zVAD (50μM) or GSK'840 (3μM) and viability was determined 14 h.p.i. HT-29 cells treated with human TNF-α (0.5ng/mL), SMAC mimetic LCL161 (5μM), and zVAD (50μM) were included as controls (TSZ). **(D)** Kinetics of cell death after wild-type or UV-inactivated (PR8 UV) PR8 infection in *ripk3*$^{+/+}$ MEFs in the presence or absence of caspase inhibitor QvD (40μM) or GSK'872 (5μM) was analyzed for up to 36 h.p.i. Cell death was determined Sytox Green uptake, and quantified as number of Sytox Green positive cells over time. **(E)** Wild-type MEFs infected with PR8 in the presence of GSK'843 (5μM), zVAD (50μM) or both inhibitors together were examined for phosphorylated MLKL or cleaved caspase 8 by immunoblot analysis at the indicated times p.i. Error bars represent mean +/− S.D. * p <0.05; ** p <0.005. See also Figs. S4 and S6.

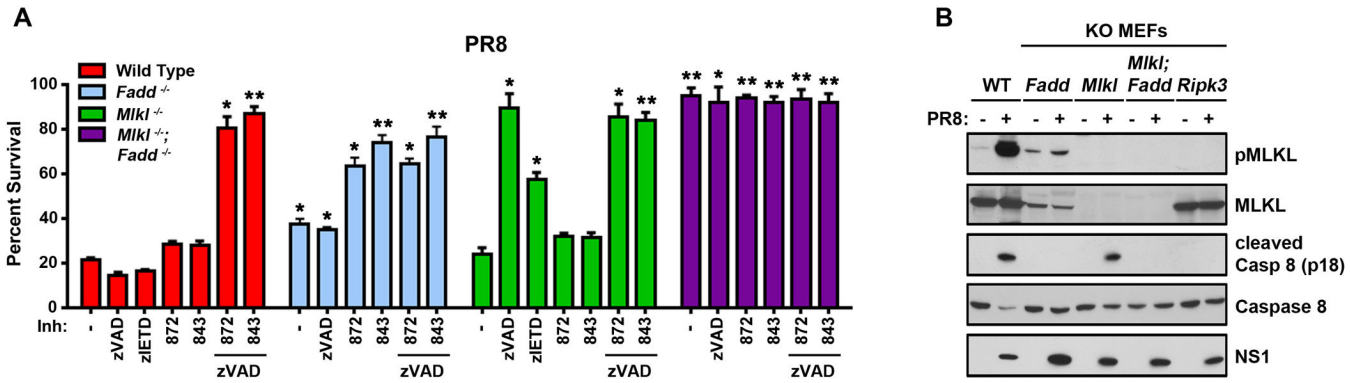

Figure 4. MLKL drives necroptosis and FADD mediates apoptosis following IAV infection

(A) Wild type, *fadd*$^{-/-}$, *mlkl*$^{-/-}$, and *mlkl*$^{-/-}$*fadd*$^{-/-}$ double knock-out MEFs were infected with PR8 in the presence or absence of pan-caspase inhibitor zVAD (50μM), the caspase 8 inhibitor zIETD (50μM) and/or 5μM of RIPK3 kinase inhibitors (GSK'872 and GSK'843). Cell viability was determined 24 h.p.i. **(B)** Wild type, *fadd*$^{-/-}$, *mlkl*$^{-/-}$ *mlkl*$^{-/-}$*fadd*$^{-/-}$, and *ripk3*$^{-/-}$ MEFs were infected with PR8 for 16 h, and examined for phosphorylated MLKL or cleaved caspase 8 by immunoblot analysis. Error bars represent mean +/− S.D. * p <0.05; ** p <0.005. See also Figs. S2, S5 and S6.

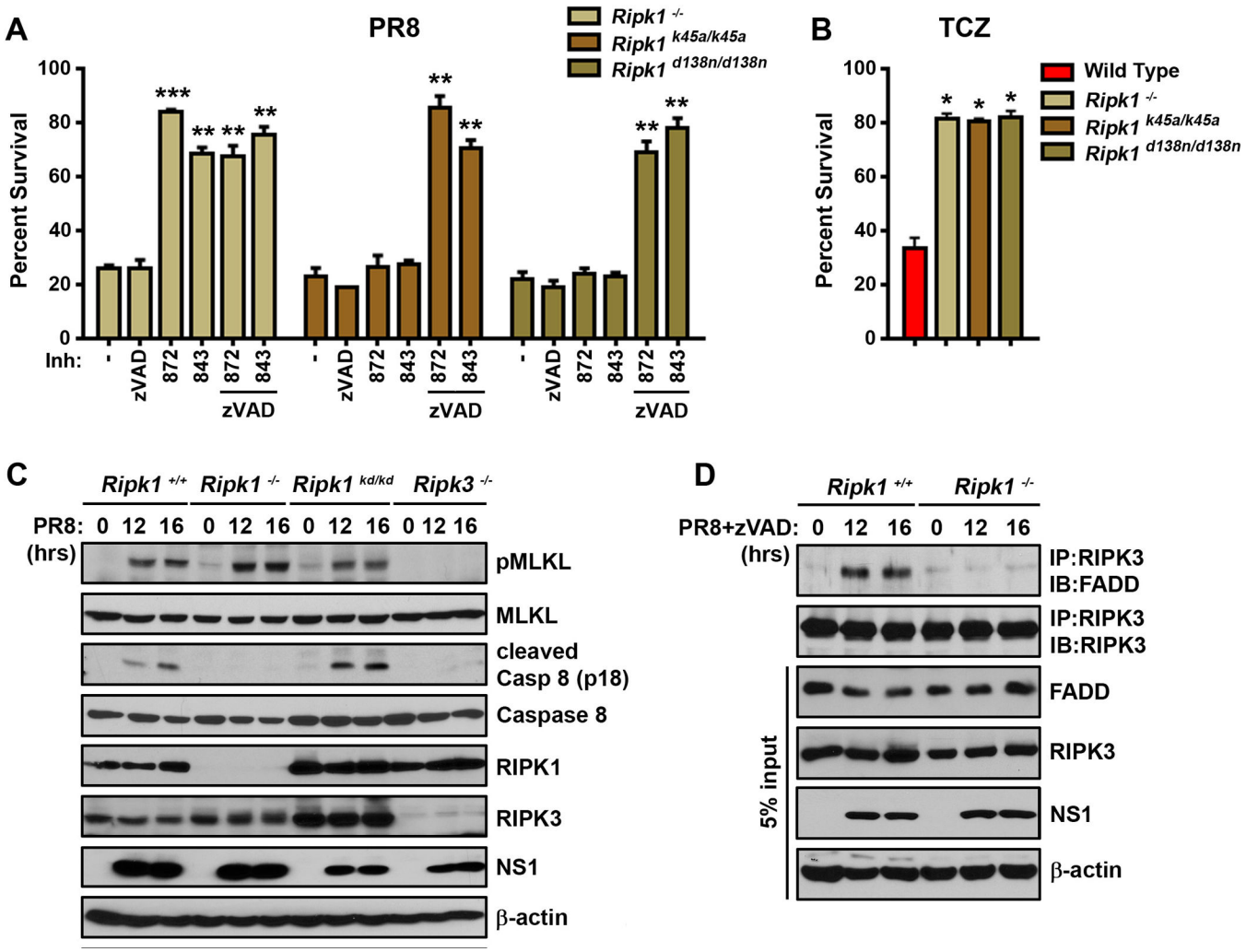

Figure 5. RIPK1 mediates RIPK3-dependent apoptosis in IAV-infected cells

(A) *Ripk1*$^{-/-}$, *ripk1*$^{k45/a/k45a}$, and *ripk1*$^{d138n/d138n}$ MEFs were infected with PR8 (m.o.i.=2) in the presence or absence of zVAD (50μM) or 5μM of the RIPK3 inhibitors GSK'872 or GSK'843, and viability was determined 24 h.p.i. **(B)** *Ripk1*$^{-/-}$, *ripk1*$^{k45/a/k45a}$, and *ripk1*$^{d138n/d138n}$ MEFs were treated with TCZ and viability was determined 24 h.p.i. **(C)** *Ripk1*$^{-/-}$, *ripk1*$^{d138n/d138n}$ (referred to as *ripk1*$^{kd/kd}$), and *ripk3*$^{-/-}$ MEFs were infected with PR8 and examined for phosphorylated MLKL or cleaved caspase 8 by immunoblot analysis at the indicated times p.i. **(D)** *Ripk1*$^{+/+}$ and *ripk1*$^{-/-}$ MEFs were infected with PR8 in the presence of zVAD (25μM). Cells were lysed at the indicated time points, and RIPK3-immunoprecipitated lysates were examined for presence of FADD. Error bars represent mean +/− S.D. * p <0.05; ** p <0.005; *** p <0.0005. See also Figs. S2 and S6.

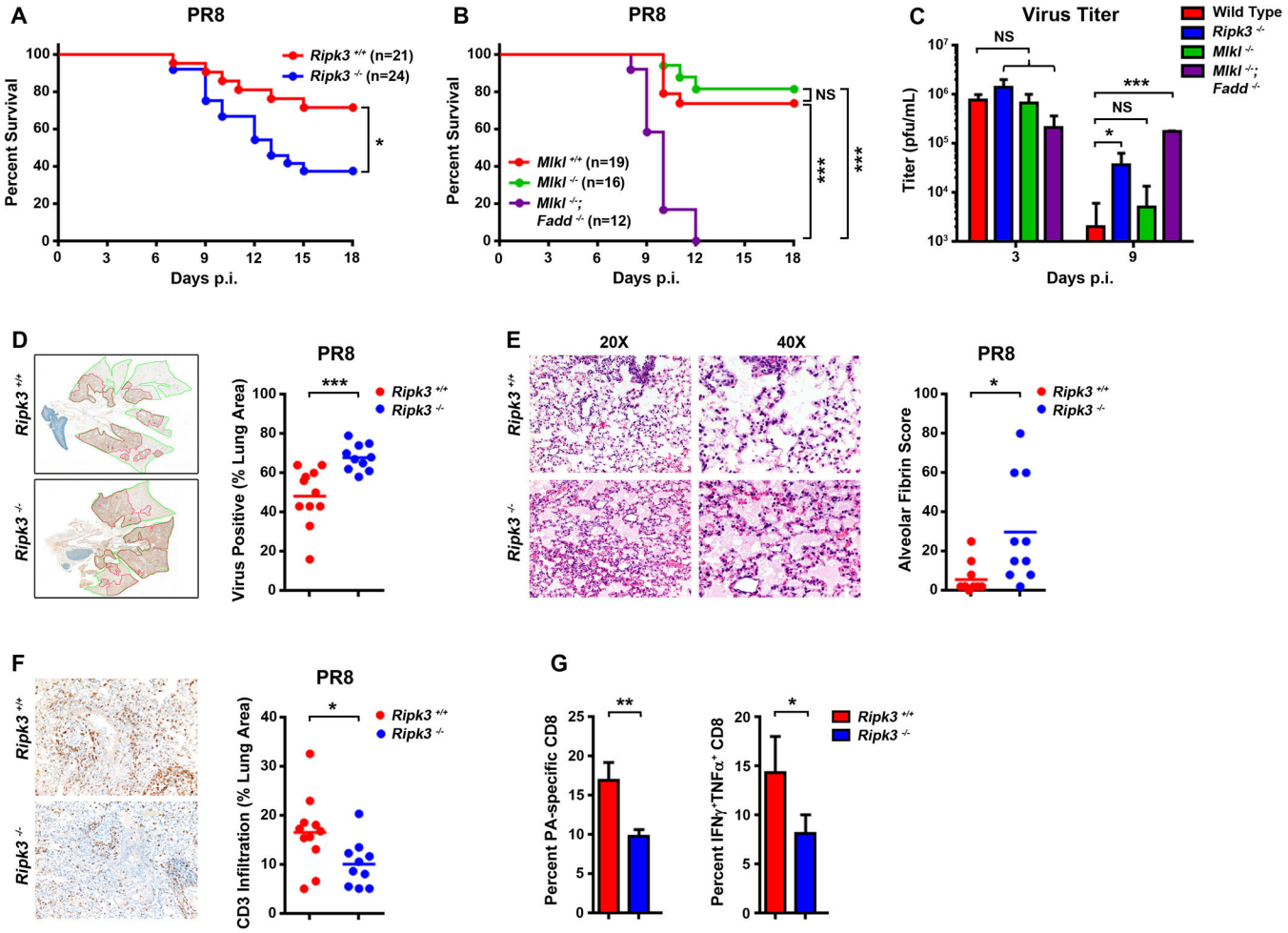

Figure 6. RIPK3-activated necroptosis and apoptosis pathways are both required for protection against IAV *in vivo*

(A) Survival analysis of age- and sex-matched *ripk3*$^{+/+}$ and *ripk3*$^{-/-}$ mice infected with PR8 (4000 EID_{50}/mouse by i.n.). **(B)** Survival analysis of age- and sex-matched *mlkl*$^{+/+}$, *mlkl*$^{-/-}$, and *mlkl*$^{-/-}$*fadd*$^{-/-}$ double knock-out mice with PR8 (4000 EID_{50}/mouse by i.n.). Data are pooled from two independent experiments. **(C)** Virus titers were determined on infected lungs 3 or 9 d.p.i. by plaque assay (n=3–5). **(D)** Paraffin embedded sections of *ripk3*$^{+/+}$ and *ripk3*$^{-/-}$ mouse lungs 6 d.p.i. were stained with anti-IAV antibodies, and slides were scanned and virus spread was quantified using Aperio ImageScope. Representative images of anti-IAV stained 11 *ripk3*$^{+/+}$ (top) and 10 *ripk3*$^{-/-}$ (bottom) lungs are shown to the left, and quantification of virus spread from lungs of individual mice are shown to the right. **(E)** Representative images of H&E-stained 11 *ripk3*$^{+/+}$ and 10 *ripk3*$^{-/-}$ lungs 6 d.p.i at two magnifications reveal severe edema and alveolar damage in *ripk3*$^{-/-}$ pulmonary tissue (left). Quantification of alveolar fibrin deposition from lungs of individual mice is shown to the right. The extent and severity of pulmonary damage was determined from blinded sections examined by a pathologist and scored for the distribution of alveolar fibrin deposition on a severity scale of 1–5. These scores were converted to a semi-quantitative scale as described previously (Matute-Bello et al., 2011). **(F)** Representative images of $CD3^+$ staining in 11

ripk3$^{+/+}$ and 10 *ripk3*$^{-/-}$ lungs 6 d.p.i. Quantification of $CD3^+$ staining from lungs of individual mice are shown to the right. **(G)** Quantification of frequencies of IAV-specific (DbPA224) $CD8^+$ T cells and percentage of IAV PA224 peptide-stimulated poly-functional IFN-γ^+TNF-α^+CD8^+ T cells in BAL fluid from *ripk3*$^{+/+}$ and *ripk3*$^{-/-}$ animals (n=3–5) at 9 d.p.i. The low pathogenic HKx31 reassortant of PR8 was used in these experiments to avoid 9 d.p.i. lethality effects seen with PR8. Error bars represent mean +/− S.D. * $p < 0.05$; *** $p < 0.0005$. See also Fig. S6.